OPEN ACCESS



Formation of the Interstellar Sugar Precursor, (Z)-1,2-Ethenediol, through Radical Reactions on Dust Grains

Juan Carlos del Valle¹, Pilar Redondo², Johannes Kästner¹, and Germán Molpeceres³

¹ Institute for Theoretical Chemistry, University of Stuttgart, Pfaffenwaldring 55, D-70569 Stuttgart, Germany; kaestner@theochem.uni-stuttgart.de

² Computational Chemistry Group, Departamento de Química Física y Química Inorgánica, Facultad de Ciencias, Universidad de Valladolid, E-47011 Valladolid, Spain

Abstract

In recent years, the continued detection of complex organic molecules of prebiotic interest has refueled the interest in a panspermic origin of life. The prebiotic molecule glyceraldehyde is proposed to be formed from (Z)-1,2-ethenediol, a molecule recently detected toward the G+0.693-0.027 molecular cloud at the galactic center. In this work, we computationally simulate the formation of (Z)-1,2-ethenediol from vinyl alcohol on the surface of amorphous solid water in a two-step synthesis involving an OH addition and an H abstraction reaction. In total, we considered all reaction possibilities of the 1,1- and 1,2-OH addition to vinyl alcohol followed by H abstraction or H addition reactions on the resulting radicals. The combination of these reactions is capable of explaining the formation of (Z)-1,2-ethenediol provided a suprathermal diffusion of OH. We also conclude that our proposed formation pathway is not selective and also yields other abstraction and addition products. Key in our findings is the connection between the adsorption modes of the reactants and intermediates and the stereoselectivity of the reactions.

Unified Astronomy Thesaurus concepts: Astrochemistry (75); Pre-biotic astrochemistry (2079); Interstellar molecules (849); Molecular data (2259); Theoretical models (2107)

1. Introduction

The formation and detection of complex organic molecules (COMs), molecules with six or more atoms, of which at least one is carbon (E. Herbst & E. F. van Dishoeck 2009), is one of the most active areas of research in modern astrochemistry. For example, one of the most striking facts in the update from the 2018 census on interstellar molecules (B. A. McGuire 2018) to the 2021 one (B. A. McGuire 2022) is the number of complex molecules involved. From all these molecules, two families are especially relevant. First, aromatic molecules (B. A. McGuire et al. 2018; J. Cernicharo et al. 2021, 2022; B. A. McGuire et al. 2021, to provide just some examples) and second, prebiotic molecules (A. Belloche et al. 2019; V. M. Rivilla et al. 2020; L. F. Rodríguez-Almeida et al. 2021; D. S. Andrés et al. 2024; V. M. Rivilla et al. 2022, 2021). Prebiotic COMs garner the attention of the astrochemical community due to the possibility of establishing a connection between the abiotic chemical space and the biotic one. In this regard, the astronomical detection of biomolecular intermediates and the elucidation of chemical pathways leading to them is especially important. So far, intermediates in the synthesis of amino acids and peptides (A. Belloche et al. 2008; V. M. Rivilla et al. 2020; L. F. Rodríguez-Almeida et al. 2021; S. Zeng et al. 2021), lipids (I. Jiménez-Serra et al. 2022; V. M. Rivilla et al. 2021), and finally sugars (V. M. Rivilla et al. 2022; S. Zeng et al. 2019) have been detected.

Focusing on the detection of the sugar precursor, our molecule of interest in this work is (Z)-ethenediol, $(Z) - HOC_2H_2OH$ (bottom leftmost structure in Figure 1),

Original content from this work may be used under the terms of the Creative Commons Attribution 4.0 licence. Any further distribution of this work must maintain attribution to the author(s) and the title of the work, journal citation and DOI.

derived from vinyl alcohol, C₂H₃OH (top leftmost structure in Figure 1). This molecule is the so-called enol form of a more stable isomer, which under Earth conditions and in equilibrium will dominate glycolaldehyde (E. E. Etim et al. 2018). However, under ISM conditions, the thermal energy is not enough to reach thermodynamic equilibrium, stimulating the spectroscopic characterization of (Z) – HOC₂H₂OH in the laboratory (M. Melosso et al. 2022), ultimately leading to its detection in the interstellar medium (ISM; V. M. Rivilla et al. 2022). Recently, the authors of the spectroscopic characterization of (Z) – HOC₂H₂OH have completed the equivalent study on the molecule's isotopologues (M. Nonne et al. 2024) The importance of intermediates like (Z) – HOC₂H₂OH in the interstellar sugar synthesis picture lies in its importance in the formose reaction, one of the oldest and most well-established chemical routes for the formation of sugars, i.e., ribose (A. Butlerow 1861; R. Shapiro 1988). It has been proposed that (Z) – HOC₂H₂OH is an ideal candidate for an equivalent of such reaction under ISM conditions through a reaction with formaldehyde (H₂CO; A. K. Eckhardt et al. 2018; M. Melosso et al. 2022). The formation of $(Z) - HOC_2H_2OH$ on interstellar ices was recently proposed through electron irradiation of CH₃OH/CO ices (N. F. Kleimeier et al. 2021). For such a route to be operative, the ice abundance of the precursors needs to be substantial, which is an easily satisfied condition in prestellar cores, where CO is completely depleted onto thick ices (P. Caselli et al. 1999). However, information on additional formation routes of sugar precursors in less-evolved molecular clouds, e.g., on purely polar amorphous solid water (ASW) ices is required to feed astrochemical models and promote further detections.

In this work, we computationally simulate the formation on interstellar dust grain analogs of (Z)-1,2-ethenediol, $((Z) - HOC_2H_2OH)$, from vinyl alcohol, (C_2H_3OH) , a

³ Departamento de Astrofísica Molecular, Instituto de Física Fundamental (IFF-CSIC), C/ Serrano 121, E-28006 Madrid, Spain; german.molpeceres@iff.csic.es

*Received 2024 May 14; revised 2024 July 31; accepted 2024 August 13; published 2024 October 9

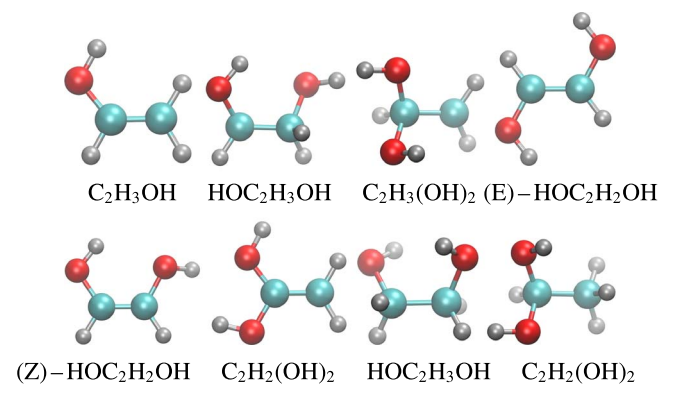


Figure 1. Gas phase structures of the molecular species involved in the reaction schemes.

molecule detected in young interstellar objects, e.g., TMC-1 (M. Agúndez et al. 2021), in a two-step synthesis involving a first OH addition followed by an H abstraction reaction. For the first reaction, we expect the 1,2 and 1,1 addition products:

$$C_2H_3OH + OH \rightarrow HOC_2H_3OH$$
 (R1)

$$C_2H_3OH + OH \rightarrow C_2H_3(OH)_2.$$
 (R2)

These reactions have been studied in the gas phase (B. Ballotta et al. 2023). In their study, the authors find the adducts HOC₂H₃OH and C₂H₃(OH)₂ submerged with respect to reactants and forming without barrier. However, subsequent evolution is either endoergic (formation of (Z)-1,2-ethenediol) or has significantly emerged barriers (formation of glycolaldehyde). Additionally, the authors study H abstraction reactions $(C_2H_3OH + OH \rightarrow C_2H_2OH + H_2O)$, finding barriers higher than in the case of the OH addition and reducing their importance for surface chemistry. Therefore, accounting for the differences in gas phase and surface chemistry on ices, we consider that formation on the grain should be feasible through H abstraction after an OH addition. Thanks to the third-body effect promoted by the interstellar ice, on the surface the additional product can stabilize and further react. We consider reactions with hydrogen for this subsequent step. Hydrogen abstraction reactions are performed on the C-H moiety, yielding (E)-1,2-ethenediol, (Z)-1,2-ethenediol and 1,1-ethenediol:

$$HOC_2H_3OH + H \rightarrow (E) - HOC_2H_2OH + H_2$$
 (R3)

$$HOC_2H_3OH + H \rightarrow (Z) - HOC_2H_2OH + H_2$$
 (R4)

$$C_2H_3(OH)_2 + H \rightarrow C_2H_2(OH)_2 + H_2.$$
 (R5)

Hydrogen addition reactions have been also considered, leading to the formation of 1,2-ethanediol (ethylene glycol, a molecule detected in the ISM (J. M. Hollis et al. 2002)), and 1,1-ethanediol:

$$HOC_2H_3OH + H \rightarrow HOC_2H_4OH$$
 (R6)

$$C_2H_3(OH)_2 + H \rightarrow C_2H_4(OH)_2.$$
 (R7)

The previous species can be found in Figure 1. In our chemical route, we propose that OH and H are the mobile reagents on the surface, meeting the other reaction partners.

In a Langmuir–Hinshelwood mechanism on interstellar dust grains, the reaction rate constant k_t , where t stands for thermal, for such a process reads (T. I. Hasegawa & E. Herbst 1993;

M. Ruaud et al. 2016):

$$k_{\rm t} = \kappa_{ij} \left(\frac{1}{\tau(i)} + \frac{1}{\tau(j)} \right) \frac{1}{N_{\rm Site} n_{\rm Dust}},\tag{1}$$

with

$$\kappa_{ij} = \frac{k_r}{k_r + k_{\text{diff}}(i) + k_{\text{diff}}(j) + k_{\text{des}}(i) + k_{\text{des}}(j)}.$$
 (2)

In the above equations, $\tau(i, j)$ are the hopping (single diffusion step) times for reactants i and j, $N_{\rm site}$ is the number of adsorption sites on a dust grain, n_{Dust} is the number density of dust grains and k_r , k_{diff} and k_{des} are the rate constants for reaction, diffusion and desorption of the species involved. From a quick inspection of Equation (1), it is clear that at least one of the reactants needs to diffuse to have a large enough rate constant for the process. This condition is satisfied for H atoms. For OH radicals, diffusion starts to be noticeable above 36 K (A. Miyazaki et al. 2022), so reactions R1 and R2 must be too slow at 10 K, as a characteristic temperature of a molecular cloud. However, in recent years, experiments have shown that, in addition to the thermal diffusion of OH, nonthermal diffusion and reaction are important promoters of interstellar chemistry (A. Ishibashi et al. 2021). Nonthermal diffusion and reaction can be triggered by a variety of actors, like photodissociation (A. Ishibashi et al. 2021) or oxygen atom hydrogenation (R. T. Garrod & T. Pauly 2011; S. Ioppolo et al. 2021). Both mechanisms generate a translationally excited OH radical (suprathermal) that can shortly overcome kinetic barriers for diffusion or reaction. The formalism for suprathermal chemistry has been developed for cosmic ray and photoninitiated chemistry (E. Mullikin et al. 2021; C. N. Shingledecker et al. 2018, 2019), but it holds for any mechanism capable of inoculating sufficient kinetic energy to freely roam the surface for a short time, like chemical energy (G. Molpeceres et al. 2023b). The rate constant k_{st} (with st referring to suprathermal) for such a process is given by (C. N. Shingledecker et al. 2018):

$$k_{\rm st} = f \left[\frac{\nu^i + \nu^j}{N_{\rm Site} n_{\rm Dust}} \right] \tag{3}$$

where f is the branching ratio, $v^{i,j}$ is the characteristic frequency of diffusion of the partners involved. The formation of a suprathermal radical that can quickly roam the surface and react for a short time is essentially equivalent to the nondiffusive mechanism postulated in Q. Chang & E. Herbst (2016), R. T. Garrod et al. (2022), M. Jin & R. T. Garrod (2020). It is important to note that the time to freely roam and react is short, because the molecule relaxes (quenches) on the surface with a rate constant equivalent to the characteristic vibrational frequency of the suprathermal species (L. D. Landau & E. M. Lifshitz 1976; C. N. Shingledecker et al. 2018):

$$k_{\rm q} = \sqrt{\frac{2N_{\rm Site}E_d}{\pi^2 m}},\tag{4}$$

where the only nondefined quantities are E_d and m are the diffusion energy and mass of the diffusing partner, OH in this case. We note that the characteristic frequencies are on the

order of 1–3 ps for molecules the size of typical interstellar molecules; and such, the quenching times are coherent with dissipation times of excess energy reported in the literature (S. Ferrero et al. 2023; G. Molpeceres et al. 2023b; S. Pantaleone et al. 2020, 2021). Although suprathermal OH can roam and react, a necessary condition for the application of Equation (3) in astrochemical models is that the inoculated energy is sufficiently large to consider the otherwise activated processes effectively barrierless. This is a trivial condition for cosmic ray-induced chemistry, as the deposited energy is enormous. For photoprocesses and chemical energy, some limited cases may exist, and computational simulations such as the ones in this work are pivotal to identifying them.

This paper is divided as follows. In Section 2 we discuss the methods that we use to construct our theoretical ice models and how we study the subsequent reactions. In Section 3 we present the the results of our work. In Section 4 we discuss our findings and contextualize the results, focusing on the isomerism of the reactions and the possible astrochemical avenues that our study opens. We conclude our work with a very brief summary of our findings.

2. Methods

We simulate amorphous solid water (ASW) using two cluster models, one consisting of $18~H_2O$ molecules and another one consisting of $33~H_2O$ molecules featuring a pocket site (A. Rimola et al. 2018; J. Perrero et al. 2022). Several binding sites are available in these models, for example, dangling oxygen (dO) sites, which are those where the oxygen atom from the water ice acts as a hydrogen acceptor, and dangling hydrogen (dH) where water acts as the H donor. Finally, the pocket sit refers to a shallow depression on the ice surface.

We characterized the stationary points in the potential energy surfaces by using density functional theory (DFT) calculations with ORCA software (F. Neese et al. 2020). First, we studied the OH radical addition step with the MPWB1K exchange and correlation functional (Y. Zhao & D. G. Truhlar 2005), and the triple-zeta basis set def2-TZVP (MPWB1K/def2-TZVP; F. Weigend & R. Ahlrichs 2005) including the D3BJ (S. Grimme et al. 2011) dispersion correction. DFT calculations were sped up by introducing the Split-RI-J variant of the density fitting approximation for the calculation of the Coulomb part of the Fock matrix and the "chain-of-spheres" algorithm for the exchange part in the so-called RIJCOSX procedure (F. Neese et al. 2009). Artificial overbinding effects that may arise from the basis set superposition error (BSSE) are corrected with the geometrical Counterpoise Correction (gCP; H. Kruse & Grimme 2012). Therefore, the method used in this work can be abbreviated as MPWB1K-D3(BJ)-gCP/def2-TZVP. The choice of this function is justified on the basis of a benchmark testing several exchange and correlation functionals compared against the high-level results in the gas phase of B. Ballotta et al. (2023). This benchmark can be found in the

Vinyl alcohol (C_2H_3OH) has two possible rotamers, syn and trans vinyl alcohol. Early spectroscopic studies acknowledge syn- C_2H_3OH as the most stable rotamer (S. Saito 1976; M. Rodler 1985). Therefore, we proceeded with this conformation during our study and we will refer to it from now on as simply C_2H_3OH . A first optimization step for both 18 H_2O

and 33 H₂O clusters was carried out. Afterward, we placed C₂H₃OH on the surface and reoptimized this new structure: we assessed the adsorption on both dH and dO sites on the 18 H₂O cluster, leaving the pocket sampling for the 33 H₂O cluster. The pocket is described as a confinement on the surface where both adsorbates can be inserted, either forming dO or dH interactions with the surrounding water molecules. Finally, we add the OH radical onto the surface near the adsorbate and reoptimize the geometry of this guess at an internuclear distance of $\sim 3.5 \,\text{Å}$ in all cases. Using these three resulting conformations as input, we carried out relaxed geometry scans along the C-O distances to produce either HOC₂H₃OH or C₂H₃(OH)₂ radicals. Because the initial guess for the reactants is placed at a relatively short distance, the barriers emerging in our scans are purely reaction barriers, and we avoid the sampling of diffusion barriers. Hence, the activation energies reported in this paper for reactions R1 and R2, the ones reported in B. Ballotta et al. (2023), should be obtained taking as reference their structure Prc1, instead of the separated reactants, namely 1.0 kcal mol⁻¹ and 1.9 kcal mol⁻¹, for reactions R1 and R2. The stationary points along the scan trajectory are then further optimized: minima as either reactants or products and the maxima as transition states (TS). Vibrational frequencies were calculated for all optimized geometries to validate them as well as to provide the zeropoint vibrational energy (ZPVE).

Later, we test H addition and H abstraction reactions on the products of the first OH addition. For these calculations, we adopted a broken-symmetry formalism. We note that the inherent (methodological) error may be larger in the case of these reactions than in the first OH addition due to the multireference nature of the system. Considering the number of reactions, we opted for a double-zeta basis set instead (def2-SVP) to lower the computational cost while achieving reasonable accuracy. The method for the second set of reactions is therefore MPWB1K-D3(BJ)-gCP/def2-SVP. We follow the same procedure from the first reaction step, though this time producing C-H distance relaxed geometry scans for the H addition reactions and H-H scans for the H abstraction reaction. We opted to fix the atom positions of the ice slab for the reactions on the pocket to ease geometry optimizations.

Finally, binding energies (BE) are defined as the attractive interactions between an adsorbate and a surface. In our case, the different chemical species involved in the reaction schemes and our ice slabs account for the respective binding sites.

BE =
$$H_{\text{bind,Ice+Adsorbate}}^{\circ} - (H_{\text{bind,Ice}}^{\circ} + H_{\text{bind,Adsorbate}}^{\circ}).$$
 (5)

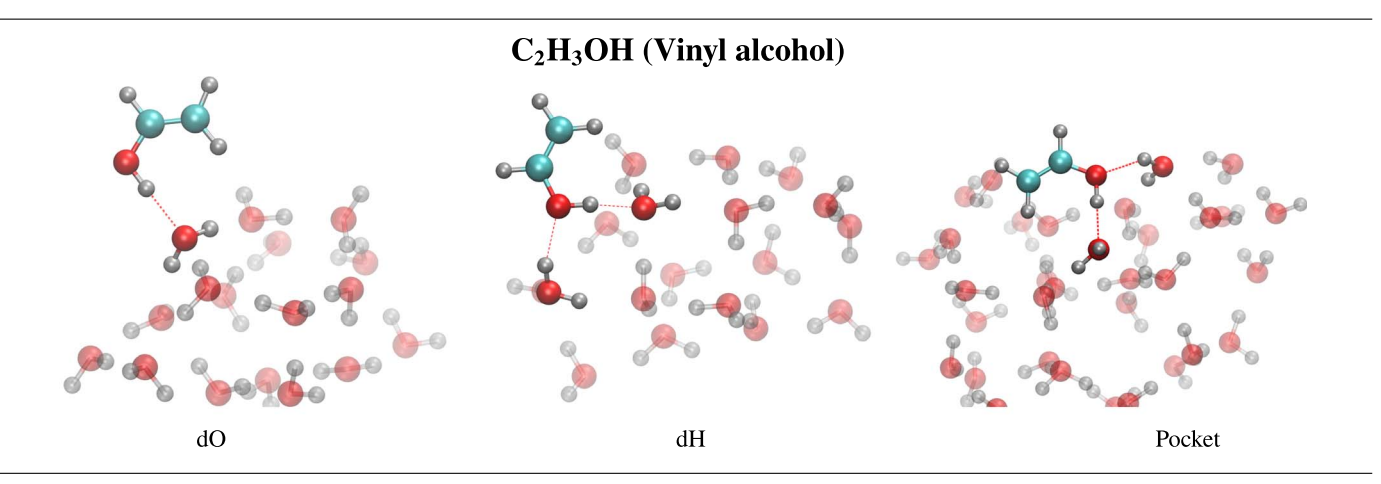
We provide individual binding energies for each molecule and binding site. These are calculated as the difference between the electronic energies, including the ZPVE of the cluster formed by the ice slab and the adsorbate in a given binding site, the ice slab, and the adsorbate in the gas phase.

3. Results

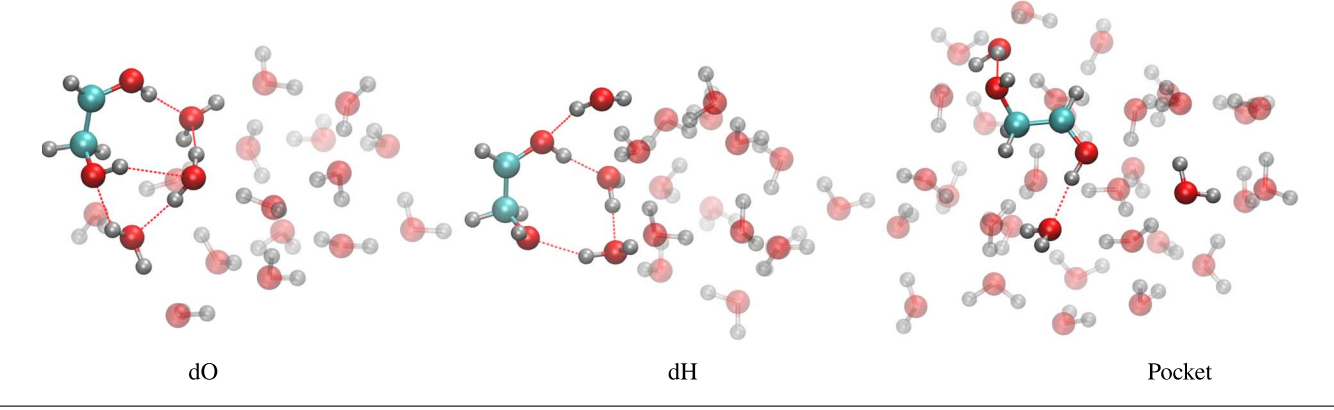
3.1. Hydroxyl Addition to C_2H_3OH

The adsorption geometries of C_2H_3OH and the products of the reaction with OH (Reactions R1 and R2) are shown in Figure 2, and BE values are gathered in Table 1.

From an analysis of the BE for C_2H_3OH (first item in Table 1 and top panel of Figure 2), we infer that, as expected, the BE strongly depends on the binding geometry (see



HOC₂H₃OH (1,2 Addition Product)



C₂H₃(OH)₂ (1,1 Addition Product)

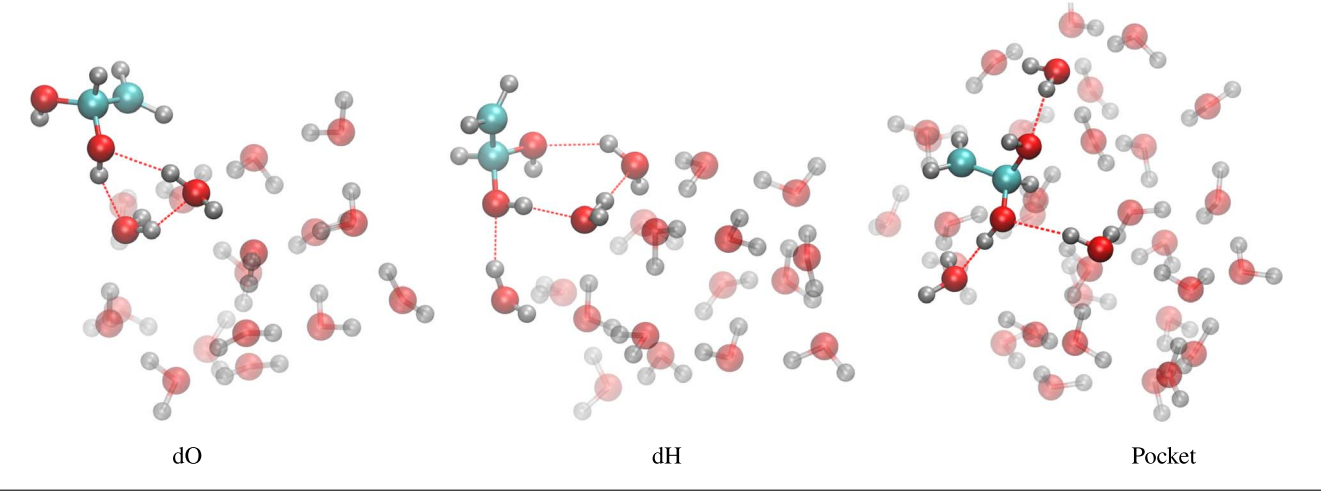


Figure 2. Adsorption geometries of vinyl alcohol (C_2H_3OH ; top panel) and its OH addition products (HOC_2H_3OH ; middle panel) and ($C_2H_3(OH)_2$; bottom panel). From left to right in each panel we show the different binding sites considered in this work, namely dO, dH, and the pocket site. The highlighted atoms in the figure indicate the adsorbate atoms and directly interacting water molecules.

Figure 3). The binding energy we found for C₂H₃OH is on par but somewhat lower than the one found for CH₃OH in the literature (S. Ferrero et al. 2020; V. Wakelam et al. 2017). Taking the study by S. Ferrero et al. (2020), the authors found that BE for CH₃OH can be found between 3770 and 8618 K as extremal values, and our values fall within this range, only slightly lower for the case of the dO binding site. The similarity in BE between C₂H₃OH and CH₃OH is expected, as both molecules are very similar. Looking at the geometric

arrangements of C_2H_3OH on the different sites, we observe that in the dH sites, the H atom of the OH group from vinyl alcohol points inward at the cluster, facilitating an arrangement of the H_2O molecules participating in the bond (top-middle panel of Figure 2). This effect fosters a unique environment at the dH sites, making them conducive to dangling hydrogen (dH) and dangling oxygen (dO) interactions. In the case of dO we do not observe such an effect, and the original site motif is maintained. Finally, it is worth remarking that while on dO and

Species	Binding Site	BE
C ₂ H ₃ OH	dO	5.6 (2808)
	dH	7.8 (3950)
	Pocket	12.5 (6315)
HOC ₂ H ₃ OH	dO	10.3 (5190)
	dH	12.5 (6272)
	Pocket	8.6 (4341)
$C_2H_3(OH)_2$	dO	7.4 (3721)
	dH	10.7 (5408)
	Pocket	11.0 (5550)
$(Z) - HOC_2H_2OH$	dO	11.4 (5733)
	dH	9.3 (4671)
HOC ₂ H ₄ OH	dO	10.9 (5466)
	dH	14.0 (7044)
	Pocket	15.4 (7762)
$C_2H_4(OH)_2$	dO	8.3 (4193)
	dH	14.9 (7505)
	Pocket	17.5 (8793)
$C_2H_2(OH)_2$	dO	12.4 (6218)
2 2\ /2	dH	9.2 (4653)
	Pocket	16.3 (8199)
$(E) - HOC_2H_2OH$	dO	5.4 (2728)
	Pocket	16.1 (8115)

dH sites the adsorption geometry is normal to the surface, on the pocket site the alcohol covers the cavity.

The energetic parameters of the reactions of OH with C₂H₃OH on the binding sites described above can be found in Table 2. In general, we observe that the values of $\Delta H^{,\ddagger}$, which is the most important quantity for reactivity, are rather in line with the gas phase values (B. Ballotta et al. 2023) both for the formation of the HOC₂H₃OH or C₂H₃(OH)₂ radicals, e.g., the H₂O surface only plays a minor catalytic role. However, and because all reactions have very low $\Delta H^{\circ, \ddagger}$ in the gas phase, we find that this minor catalytic role can make some pathways totally barrierless for the reaction R1. This is not the case for the reaction R2, where $\Delta H^{\circ, \ddagger}$ varies in the 0.9–2.1 kcal mol⁻ range. This finding can be important when considering competitive reaction channels when OH thermally diffuses on the surface at $T \ge 36$ K (A. Miyazaki et al. 2022), but in this work we are more interested in the role of suprathermal OH, where the internal energy of the radical should easily surpass $\Delta H^{\circ,\ddagger}$. We discuss this fact in more detail in Section 4, and here it suffices to say that there should not be a preferential reaction path when suprathermal OH is considered.

The structural arrangements between the adsorbate and surface produced by the reaction will eventually determine the stereoselectivity of the whole reaction path. Vinyl alcohol is a planar molecule, and so the addition of the OH radical produces a pyramidalization of the given carbon center (C sp² \rightarrow C sp³). The 1,2 OH addition on C₂H₃OH in the dO and dH sites leaves the initial hydrogen bonds unchanged, to which the newly formed OH group adds two and one new hydrogen bonds, respectively (see the middle panels of Figure 2). Restructuring HOC₂H₃OH for the 1,2 addition on the pocket binding site is more complicated. The addition distorts the molecule so that

the initial hydrogen bond bonded by the dH site breaks, and a new dH site hydrogen bond is formed through the newly added OH group. We observe that the two OH groups are staggered and that one hydrogen atom bonded to the sp³ carbon is forced to rotate into the pocket. This is essential for the following H abstraction reaction, as it leads to only (E)-1,2-ethenediol.

The formation of $C_2H_3(OH)_2$ radical (geminal addition to C₂H₃OH) always proceeds with the formation of new hydrogen bonds. In the dO site, we observe a cleavage of the original hydrogen bond to form a new hydrogen bond with a neighbor H₂O molecule, followed by a restructuring of the dO water site, with the -OH moiety of C₂H₃(OH)₂ acting both as H donor and acceptor (Lower left corner of Figure 2). Besides, the newly added OH group does not interact with the ice slab. Meanwhile, in the dH and pocket sites, the new OH group interacts with the ice, furnishing one new hydrogen bond in each case. Furthermore, the interactions within the pocket force, as in the HOC₂H₃OH case presented above, a motion in the hydrogen atom bonded to the sp³ carbon inward at the cluster, with important consequences for the subsequent stereoselectivity of the H abstraction. Besides, the torsional angle HCCH is shifted, making the gas phase and the adsorbed-phase minimum energy conformations diverge. This will have further implications in

The variations in the BE of the newly formed radicals are related to the creation or breaking of hydrogen bonds due to the addition of OH as the molecules accommodate on the surface. In absolute terms, the BE of radicals is on par with other molecules susceptible to forming H bonds with the surface, such as CH₃OH (S. Ferrero et al. 2020), HCOOH (G. Molpeceres et al. 2022) or NH₂OH (G. Molpeceres et al. 2023a), e.g., close to the BE of H₂O on the same substrate (L. Tinacci et al. 2023).

3.2. H Abstraction and Addition Reactions from OH Addition Products

The hydrogen abstraction from OH addition products (Section 3.1) leads to the exothermal formation of unsaturated diols. From HOC_2H_3OH we may obtain (E) $-HOC_2H_2OH$ and (Z) $-HO_2C_2H_2OH$ depending on the binding site. Starting from $C_2H_3(OH)_2$, we can produce only $C_2H_2(OH)_2$ (e.g., no stereoisomerism).

A summary of the energies for the reaction with H is shown in Table 3. From it, we observe that the formation of the 1,1 products is consistently more exothermic than that of the 1,2 products, regardless of the binding site. Moreover, H abstraction reactions on the dO site are more exothermic than those on the dH sides. We found all H abstraction and addition reactions barrierless, except reaction R4, which proceeds with a small barrier of $\Delta H^{\circ,\ddagger} = 1.0 \, \text{kcal mol}^{-1}$.

The formation of $(Z) - HOC_2H_2OH$ is possible on binding sites dH and dO, and $(E) - HOC_2H_2OH$ on dO sites and the pocket site as no barrier is expected (see Table 3). We also observe that the sites where $(Z) - HOC_2H_2OH$ is formed are consistent with those where the binding energies of the precursor HOC_2H_3OH are highest. On the dH site, the strong hydrogen bonds acting on both OH groups in HOC_2H_3OH force them toward the ice surface throughout the H abstraction process, as observed in Figure 4, so that H abstraction leads to $(Z) - HOC_2H_2OH$ exclusively. The weaker interaction on the dO site means that molecules here will have more freedom to rearrange, yielding both $(Z) - HOC_2H_2OH$ or

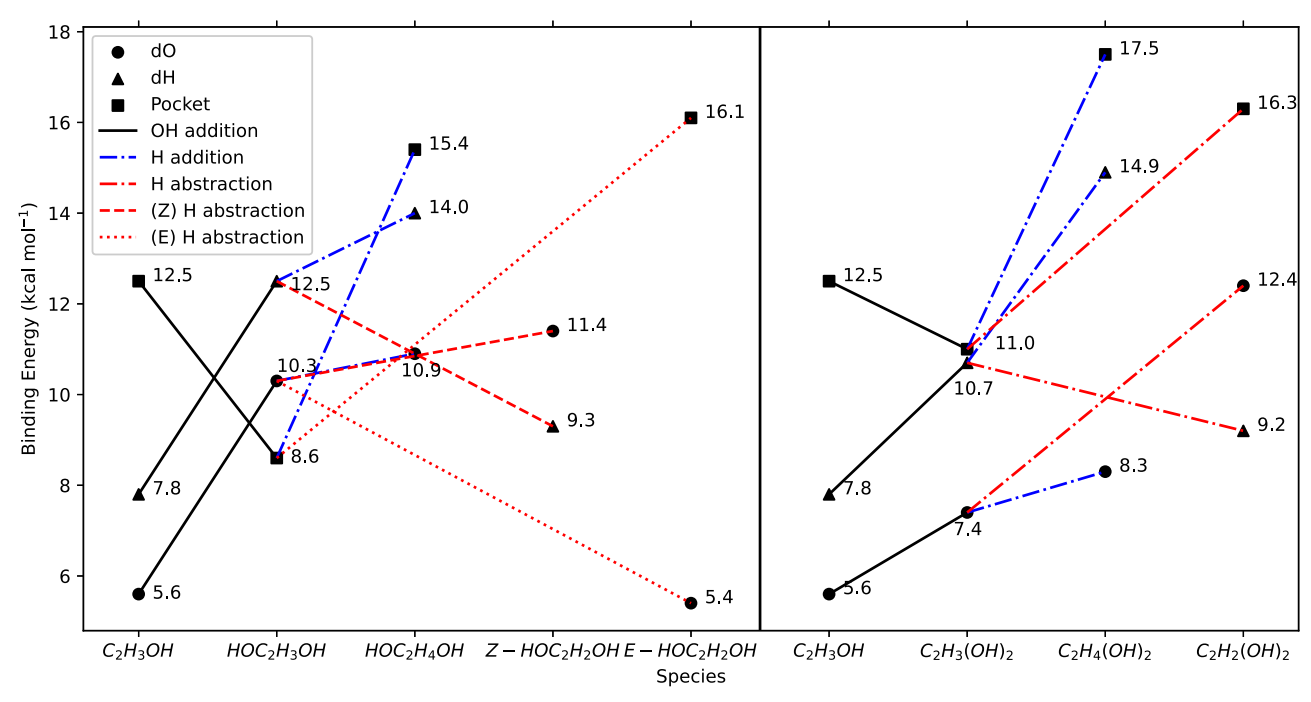


Figure 3. Evolution of the binding energies of the species on the different binding sites. The left-hand side of the figure features the species that evolved from the 1,2 addition of OH to C_2H_3OH , and on the right-hand side, those that evolved from the 1,1 addition.

(E) - HOC₂H₂OH. The case of the pocket is straightforward as the OH groups in HOC₂H₃OH are already in a staggered position, and only the H atom on top may be abstracted, leading to the (Z) - HOC₂H₂OH. These facts can also be observed in Figure 5, which shows a close-up view of the reactions.

We acknowledge that in gas phase $(Z) - HOC_2H_2OH$ can be present as conformer (Z)-(syn,anti) and (Z)-(anti,anti), and $(E) - HOC_2H_2OH$ as (E)-(syn,syn), (E)-(syn,anti) and (E)-(anti,anti) regarding the rotation of the alcohol groups. The energy difference between the first two is in the order of 4.1 kcal mol⁻¹, whereas the differences between (E)-(syn,syn), (E)-(syn,anti) and (E)-(syn,anti), (E)-(anti,anti) are 0.5 and 0.2 kcal mol⁻¹ respectively (N. F. Kleimeier et al. 2021). In our study we observed isomer (E)-(syn,anti) on a dO site and (E)-(syn,syn) in the pocket, whereas only the (Z)-(syn,anti) was observed regardless of the binding site (see Figure 4). The low energy difference in the conformations of the (E)-isomer makes us consider unimolecular isomerization once released to the gas phase as a possible outcome on astronomical timescales, which can affect the detectability of the molecule. In the case of the (Z)-conformer, the high activation energy precludes this interconversion, making the conformer desorbing from the grain the one to be detectable. This is an important aspect to consider when envisaging new astronomical detections of these unsaturated species.

Reaction $\hat{R}5$ is barrierless and exothermic in all binding sites, as shown in Table 3. Moreover, there is a generalized increase of the BE comparing those of $C_2H_3(OH)_2$ and $C_2H_2(OH)_2$ except on the dH site (as seen in Figure 3).

The hydrogen addition to HOC_2H_3OH and $C_2H_3(OH)_2$ takes place at the formal sp^2 carbon atom, yielding HOC_2H_4OH , ethylene glycol, and $C_2H_4(OH)_2$, respectively. All reactions are exothermic and barrierless. Reaction R7 is more exothermic than Reaction R6 in all binding sites. As we mentioned in Section 3.1, Reaction R5 is also more exothermic than Reactions R3 or R4. Moreover, in the general picture, we

observe very small energy differences in the different binding sites, with slightly higher values in dH sites. The adsorption geometries of the H addition reaction products are shown in Figure 6.

4. Discussion

4.1. Isomerism

Our calculations show that the formation of $(Z) - HOC_2H_3OH$ from C_2H_3OH is indeed feasible through the action of OH and H radicals on the surface of interstellar dust grains, and that the barriers that need to be overcome are, in all cases, lower than the corresponding thermal diffusion barriers of the reactants involved. We thus expect the formation of isomers (E) and $(Z) - HOC_2H_2OH$ as well as the H addition products (HOC_2H_4OH) , the saturated and unsaturated geminal diols $(e.g., R - (OH)_2)$

The most important point of our work is validating a postulated chemical reaction pathway for the formation $(Z) - HOC_2H_3OH$, as its recent detection (V. M. Rivilla et al. 2022) prompted some questions about chemical isomerism in space. Quantum tunneling mediated unimolecular interconversion has recently been able to explain the thermodynamic isomeric ratio of imines (J. García De La Concepción et al. 2021), though failing to explain the case of formic acid (HCOOH; J. García de la Concepción et al. 2022). The case of $(E) - HOC_2H_2OH \Rightarrow (Z) - HOC_2H_2OH$ requires an unfeasible torsion through a double bond, making this mechanism inoperative though leaving the door open to photon-mediated processes (S. Cuadrado et al. 2016) or chemical conversion in gas or grains (G. Molpeceres et al. 2022; C. Shingledecker et al. 2020; J. García De La Concepción et al. 2023)

The diffusion energies of C_2H_3OH and related species are not known, but in light of the high ΔH_{bin}° listed in Table 1, it is safe to assume that they will be immobile.

Label	Reaction	Binding Site	$\Delta H^{\circ,\mathrm{R}}$	$\Delta H^{\circ,\ddagger}$
R1	$C_2H_3OH + OH \rightarrow HOC_2H_3OH$	dO	-27.5 (-31.6)	BL
R1	$C_2H_3OH + OH \rightarrow HOC_2H_3OH$	dH	-25.4 (-28.2)	0.3 (0.5)
R1	$C_2H_3OH + OH \rightarrow HOC_2H_3OH$	Pocket	-22.6 (-27.6)	BL
R2	$C_2H_3OH + OH \rightarrow C_2H_3(OH)_2$	dO	-26.3 (-28.4)	0.9 (0.4)
R2	$C_2H_3OH + OH \rightarrow C_2H_3(OH)_2$	dH	-25.1 (-26.4)	2.1 (2.6)
R2	$C_2H_3OH + OH \rightarrow C_2H_3(OH)_2$	Pocket	-23.5 (-25.5)	1.4 (1.0)

Note. Energies are ZPVE corrected. In parentheses, electronic energies, e.g., without ZPVE. All values are reported in kcal mol⁻¹. BL stands for barrierless. As a reference, the activation energies in the gas phase from the Prc1 complex, reported in B. Ballotta et al. (2023), are 1.0 kcal mol⁻¹ for reaction R1 and 1.9 kcal mol⁻¹ for reaction R2.

Table 3
Summary of the Reaction Energies $\Delta H^{\circ,R}$ and Activation Energies $\Delta H^{\circ,\ddagger}$ for the Second Hydrogenation Step Studied in This Work

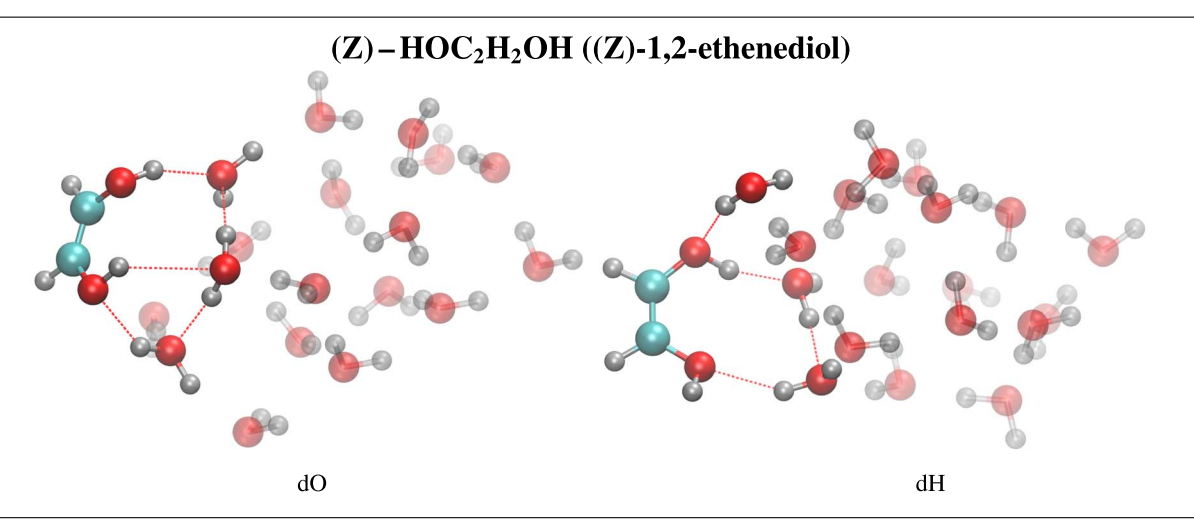
Label	Reaction	Binding Site	$\Delta H^{\circ,\mathrm{R}}$	$\Delta H^{\circ,\ddagger}$
R3	$HOC_2H_3OH + H \rightarrow (E) - HOC_2H_2OH + H_2$	dO	-60.7 (-61.2)	BL (0.6)
R4	$HOC_2H_3OH + H \rightarrow (Z) - HOC_2H_2OH + H_2$	dO	-66.2 (-66.8)	BL
R6	$HOC_2H_3OH + H \rightarrow HOC_2H_4OH$	dO	-84.5 (-94.2)	BL
R5	$C_2H_3(OH)_2 + H \rightarrow C_2H_2(OH)_2 + H_2$	dO	-82.4 (-80.8)	BL
R7	$C_2H_3(OH)_2 + H \rightarrow C_2H_4(OH)_2$	dO	-97.7 (-107.3)	BL
R4	$HOC_2H_3OH + H \rightarrow (Z) - HOC_2H_2OH + H_2$	dH	-61.0 (-62.0)	1.0 (0.9)
R6	$HOC_2H_3OH + H \rightarrow HOC_2H_4OH$	dH	-85.5 (-94.4)	BL
R5	$C_2H_3(OH)_2 + H \rightarrow C_2H_2(OH)_2 + H_2$	dH	-72.1 (-72.5)	BL (0.5)
R7	$C_2H_3(OH)_2 + H \rightarrow C_2H_4(OH)_2$	dH	-99.6 (-108.0)	BL
R3	$HOC_2H_3OH + H \rightarrow (E) - HOC_2H_2OH + {H_2}^*$	Pocket	-64.8 (-64.0)	BL (1.4)
R6	$HOC_2H_3OH + H \rightarrow HOC_2H_4OH^*$	Pocket	-85.1 (-93.8)	BL
R5	$C_2H_3(OH)_2 + H \rightarrow C_2H_2(OH)_2 + H_2^*$	Pocket	-73.7 (-75.5)	BL
R6	$C_2H_3(OH)_2 + H \rightarrow C_2H_4(OH)_2^*$	Pocket	-98.3 (-107.3)	BL

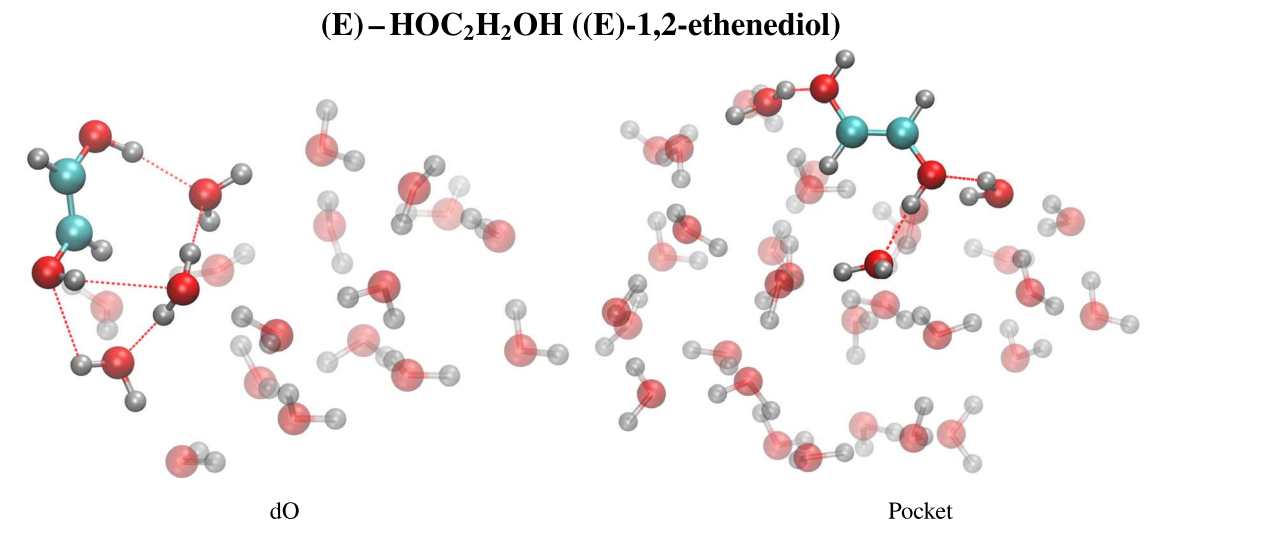
Notes. Energies are ZPVE corrected. In parentheses, electronic energies, e.g., without ZPVE. All values are reported in kcal mol⁻¹. BL means barrierless. (*) Ice slab with fixed atoms. See Section 2 (**) Computed with broken-symmetry DFT. A larger uncertainty in $\Delta H^{\circ,R}$ and $\Delta H^{\circ,\ddagger}$ is expected with respect reactions R1 and R2.

As we already mentioned, the formation of (Z) – HOC₂H₂OH is possible, but further reactions are competitive. Hence, a more detailed discussion is required in order to facilitate subsequent astronomical searches. The occurrence of one or another reaction depends mostly on the binding site on ASW, which, as we found in earlier works (G. Molpeceres 2021a; G. Molpeceres et al. 2022), modulates the stereochemistry based on the hydrogen bond topology of the adsorbate (C₂H₃OH as a precursor in this case), with the surface. Another plausible competitive reaction would be the hydrogenation of C_2H_3OH , leading to the formation of ethanol. This was previously studied by J. Perrero et al. (2022) in a very similar fashion to that of our study by employing ASW clusters. Both possible additions, either on the aliphatic carbon or the OH-bearing one, were reported to proceed with small barriers that could be overcome by quantum tunneling. These reactions will compete with the first step of our proposed scheme and, due to the flux of H atoms impinging on interstellar ASW, possibly dominate. This is coherent with the expected abundances of ethanol, an ice molecule recently detected by JWST observations (W. R. M. Rocha et al. 2024), that should be much more abundant than our title molecule. The presence of competitive hydrogenation routes at low temperatures, however, does not preclude our proposed route. Our route at low temperatures is also enhanced by H accretion on ices, for example through a three-body mechanism where a

suprathermal OH radical can diffuse and react with a nearby C_2H_3OH molecule (R. T. Garrod & T. Pauly 2011; M. Jin & R. T. Garrod 2020; R. T. Garrod et al. 2022), with evidence for this process to occur in the presence of available hydrogenation channels (Q. Chang & E. Herbst 2016; A. Ishibashi et al. 2021).

We emphasize again that our discussion so far pertains to the chemistry at low temperatures (e.g., 10 K) where the OH radical participating in the first reaction $C_2H_3OH + OH$, is excited by different mechanisms, such as, for example, water photolysis (A. Ishibashi et al. 2021) or transient heating after a reactive event $O + H \rightarrow OH^*$ (see, e.g., R. T. Garrod & T. Pauly 2011). Because of the attenuation of the primary interstellar UV field, photolysis is not expected to contribute a lot to the generation of OH radicals in molecular clouds. Making this physical regime suitable for the reactions studied in this work. Assuming that the kinetic barriers found in Table 2 can be overcome suprathermally as well, we see that all products of reactions R1 and R2 must be equally possible. We do not observe any preferential chemistry because suprathermal rate constants are barrier and temperature independent; see Equation (3) and C. N. Shingledecker et al. (2018). A posterior reaction with H also shows no or minute barriers (easily passed via quantum tunneling) for concluding the reaction (reactions R3-R7; Table 3). Although in this case we do observe preferential stereochemistry based on the hydrogen bond





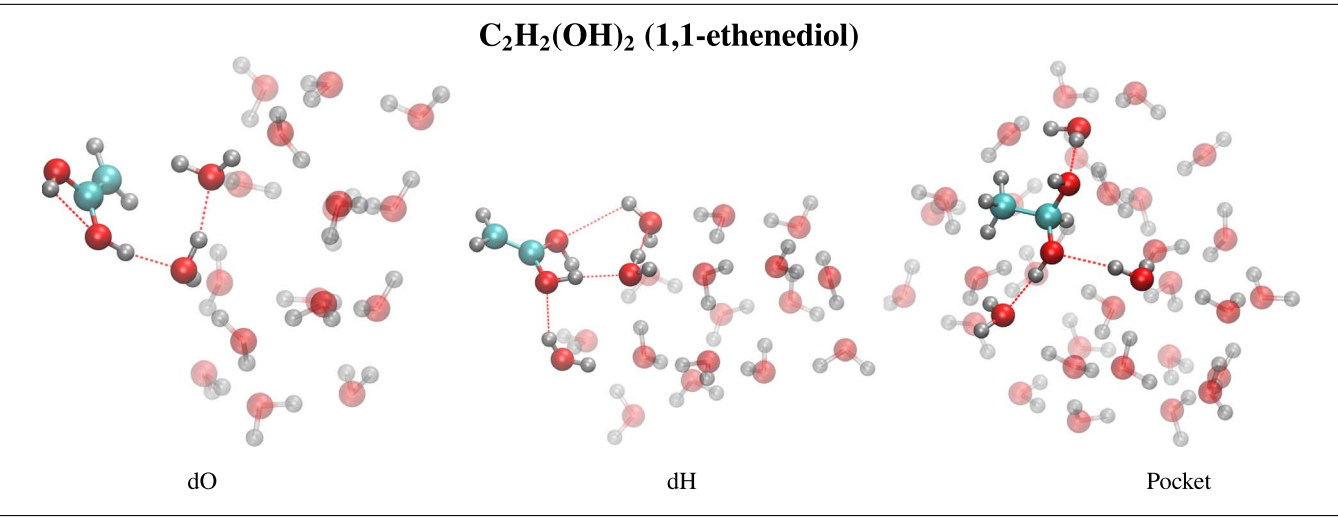
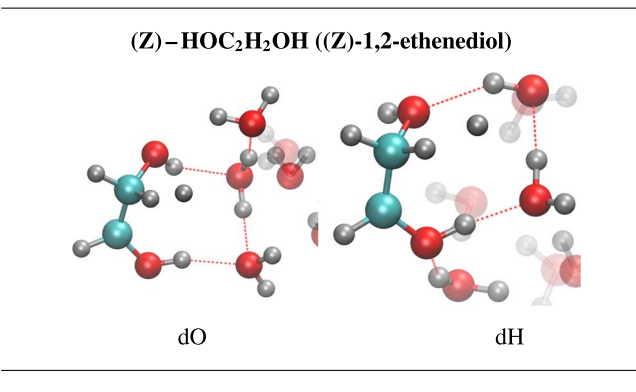


Figure 4. Adsorption geometries of (Z)-1,2-ethenediol ((Z) - HOC₂H₂OH; top panel), (E)-1,2-ethenediol ((E) - HOC₂H₂OH; middle panel) and 1,1-ethenediol (C₂H₂(OH)₂; bottom panel). From left to right in each panel we show the different binding sites considered in this work, namely dO, dH, and the pocket site. The highlighted atoms in the figure indicate the adsorbate atoms and directly interacting water molecules.

topology of the preadsorbed reactant, a mixture of all products of the reaction shown in reactions R3–R7 can be possible, with specific abundances depending on the distribution of binding sites on the surface.

A second regime starts when two conditions are satisfied. First, the H atom population on the surface is negligible due to thermal evaporation (at $\sim \! 18 \, \mathrm{K}$), and OH radicals start to be mobile (36 K, A. Miyazaki et al. 2022). The evaporation of H



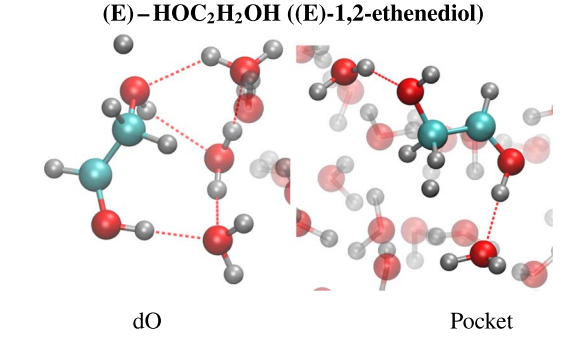


Figure 5. Close-up snapshots of the H abstraction process leading to different stereoisomers on selected binding sites. The top panel corresponds to $(Z) - HOC_2H_2OH$ and the bottom panel corresponds to $(E) - HOC_2H_2OH$.

atoms inhibits the formation of suprathermal OH* and reaction R3–R7, making thermal diffusion the limiting step for the reaction and H abstraction reactions to proceed *via* alternative reactants (i.e., OH, NH₂; not considered in this work). Under this regime, we expect that the barrierless or low barrier channel to form the 1,2 product (Reaction R1) dominates. This second regime is temperature dependent because both reactions R1 and R2 now follow Equation (1).

In light of this discussion, we consider that, in the absence of a direct isomerization mechanism in the gas, that is, S. Cuadrado et al. (2016), J. García De La Concepción et al. (2021) or J. García De La Concepción et al. (2023) or a clearly favored reaction route for the stereochemistry of the reaction (G. Molpeceres 2021a) it is very complicated to determine the isomerism of a gray case like the one tackled in this article. The specific isomeric excess depends on the binding site and the temperature window. This is the second important point extracted from this work. Sophisticated chemical modeling efforts are required to quantify the importance of every isomer, structural and spatial, in the total scheme of the reaction. We postpone such a study for future works. A similar speciation of possible isomers was found in the electron irradiation experiments of N. F. Kleimeier et al. (2021), with the inclusion of even further products, e.g., 1-3-oxyranol, due to the high energy dose inoculated in their experiments.

4.2. Astrochemical Rationale: New Molecules Proposed for Detection

So far, the molecule under scrutiny in this work, $(Z) - HOC_2H_2OH$ has been detected only in the giant molecular cloud G+0.693-0.027, at the center of our galaxy, contrary to the lower energy isomer, glycolaldehyde, that has

been detected in more than one source (M. T. Beltrán et al. 2008; J. M. Hollis et al. 2000; J. K. Jørgensen et al. 2012; A. Coutens et al. 2015). In their work, V. M. Rivilla et al. (2022) suggest five different routes for the formation of (Z) – HOC_2H_2OH , namely the H_2CO/CH_2OH pair, dimerization of hydroxycarbene (HCOH), hydrogenation of glyoxal HCOCHO, enolisation of glycolaldehyde (HCOCH₂OH) and the route that we considered in this work, hydroxylation of vinyl alcohol (C_2H_3OH) followed by a hydrogen abstraction reaction. From all the possible reaction routes, we believe that the one considered in this work is the most plausible one, owing to chemical considerations affecting the alternatives that we enumerate below.

Beginning with the dimerization of HCOH, we recently showed that this species undergoes quick conversion to H₂CO on polar ices through efficient proton relay mechanisms (G. Molpeceres et al. 2021b). While we found this phenomenon to be binding site dependent, we find it difficult to consider that, given this reactivity, to have two close HCOH molecules together on a dust grain under ISM conditions. By contrast, reactions of HCOH in the gas phase, where reaction with the ice mantle is not possible, are reported to be crucial in the synthesis of sugars (A. K. Eckhardt et al. 2018). Second, the HCOCHO + 2H route was already studied in the literature, finding significantly easier hydrogenation at the C position toward the H₂COCHO radical (S. Álvarez Barcia et al. 2018), precluding the formation of HOC₂H₂OH. Third, the enolisation of glycolaldehyde is an unimolecular-activated and endothermic process, not feasible under ISM conditions. Therefore, only $H_2CO + CH_2OH + 2H$ and our proposed route $C_2H_3OH + OH + H$ remain viable candidates. We carried out additional gas phase calculations (at the same MPWB1K-D3 (BJ)/def2-TZVP level) on the $H_2CO + CH_2OH$ reaction, finding a barrier of $\sim 5.0 \text{ kcal mol}^{-1}$, i.e., a sizable barrier. Following the arguments given in this article, such a barrier might be overcome suprathermally, although in this case suprathermal diffusion is a competitive process. Comparing H₂CO (or CH₂OH) with OH, the higher number of degrees of freedom of these polyatomic molecules does not allow for similarly efficient excitation of translational degrees of freedom. In fact, while A. Ishibashi et al. (2021) reported the presence of suprathermal OH, a similar behavior has not been found for bigger molecules.

Overall, based on pure chemical arguments, our route is the most promising one, although C₂H₃OH is the least abundant of the C₂H₄O family of molecules, at least in Sgr-B2 (A. Belloche et al. 2013), IRAS 16293-2422 (J. M. Lykke et al. 2017) or astrochemical models (R. T. Garrod et al. 2022). However, recent theoretical calculations show new and efficient routes for the formation of vinyl alcohol (G. Molpeceres & V. M. Rivilla 2022; J. Perrero et al. 2022) summed to studies addressing the limited resilience of C₂H₃OH in the gas phase (B. Ballotta et al. 2023) suggest that the abundance of C₂H₃OH in grains can be larger than expected, serving as feedstock to more complex prebiotic COMs. In this work, we anticipate some of these COMs as not only $(Z)-HOC_2H_2OH$ but also (E)-HOC₂H₂OH, HOC₂H₄OH, C_2 H₄(OH)₂ and C_2 H₂(OH)₂. In the absence of destruction routes operating in these molecules that are beyond the scope of this work, we expect these molecules to be detectable in the ISM and encourage laboratory work informing about the necessary spectroscopic parameters conducive to their detection.

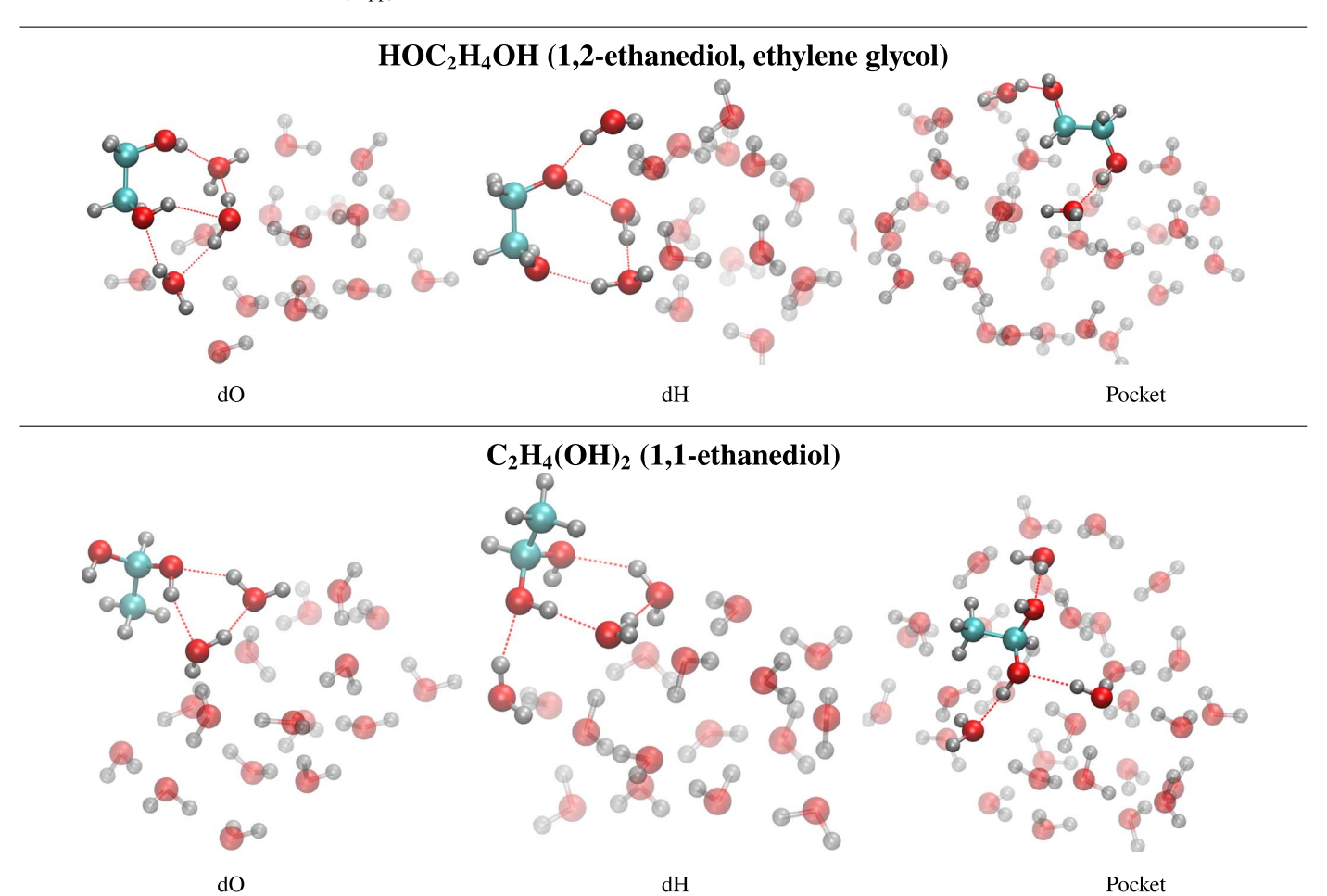


Figure 6. Adsorption geometries of 1,2-ethanediol (ethylene glycol, HOC_2H_4OH ; top panel) and 1,1-ethanediol $(C_2H_4(OH)_2)$; lower panel). From left to right in each panel we show the different binding sites considered in this work, namely dO, dH, and the pocket site. The highlighted atoms in the figure indicate the adsorbate atoms and directly interacting water molecules.

Finally, it remains to understand why $(Z) - HOC_2H_2OH$ has so far only been detected in G+0.693-0.027. Although giving a definitive explanation is extremely difficult, we believe that the distinctive chemistry operative in this astronomical object is a very important factor. So far, the chemistry of G+0.693-0.027 hints at an important contribution of surface chemistry to the molecular inventory of the cloud, not only with (Z) - HOC₂H₂OH but also with, i.e., with HC(O)SH (L. F. Rodríguez-Almeida et al. 2021), NH₂OH (V. M. Rivilla et al. 2020) or very recently HOCOOH (M. Sanz-Novo et al. 2023) or HNSO (M. Sanz-Novo et al. 2024). Some of these products' chemistry can be explained by hydrogenations (G. Molpeceres 2021a; G. Molpeceres et al. 2023a), but some others necessitate the diffusion of heavier radicals to proceed. While some of these radicals, like the N or O atoms, might diffuse on ASW at \sim 10–15 K (M. Minissale et al. 2013, 2016; V. Zaverkin et al. 2022), others are immobile (OH as an example in this work), and nonthermal diffusion and reaction needs to be invoked. G+0.693-0.027, with an extremely high flux of cosmic rays (M. Goto 2014) or cloud-cloud collisions (S. Zeng et al. 2020), provide the necessary energy to put these energetic phenomena at the forefront of the observed chemical complexity. Further investigation of unconventional chemical routes that can operate in this source is in our immediate plans. The particular

conditions of G+0.693-0.027 are not only ideal for our proposed chemical route but also for the radiolytic route presented by N. F. Kleimeier et al. (2021), reinforcing the view of G+0.693-0.027 as a factory of prebiotic COMs.

5. Conclusions

The current study sheds light on the reactivity of vinyl alcohol on ASW surfaces and its role in the synthesis of the sugar precursor (Z) - HOC₂H₂OH, highlighting the effect of the binding configurations on the stereoselectivity of the reactions. Our quantum chemical calculations show that all the reactions participating in the chemical scheme under consideration are barrierless or possess rather low barriers, with a couple of exceptions on particular binding sites. Even for exceptions, all activation energies are lower than the diffusion barrier for the OH radical, hence confirming that suprathermal OH must readily react with C₂H₃OH. Our simulations also provide valuable information on the BE of all the species involved in our reaction scheme, as well as variations during the reaction and reaction energies. These quantities can be directly included in astrochemical models looking to reproduce the abundances of (Z) - HOC₂H₂OH in interstellar environments, an endeavor that we will pursue with further dedicated works.

In addition to the finding of kinetic barriers or lack thereof for our postulated chemical scheme, our work also focuses on the isomerism of the considered reactions. Through the analysis of the binding of the reactants to the surface, we are able to determine that the formation of $(Z) - HOC_2H_2OH$ is not isomerically pure. In fact, the extreme reactivity exhibited by all the reactants and intermediates considered makes us conclude that all possible products of the reaction involving stereoisomers (e.g., $(E)-HOC_2H_2OH)$, structural isomers $(C_2H_2(OH)_2)$ or addition products (molecules with formula C_2H_2OH). We suggest that these molecules are good candidates for spectroscopic and interstellar search, at least in sources with a low dust temperature (10-18 K, See Section 4.1)

In conclusion, our research offers extensive data on the formation of sugar precursors in molecular clouds. We underscore the importance of the molecular interactions with the ASW surface as they dictate the selectivity of the reactions. Likewise, we encourage further experimental, theoretical, and modeling studies to keep growing the astrochemical knowledge on reactions with the OH radical once its mobility has been proven due to nonthermal effects (A. Ishibashi et al. 2021).

Acknowledgments

This work was funded by Deutsche Forschungsgemeinschaft (DFG, German Research Foundation) under Germany's Excellence Strategy - EXC 2075 - 390740016. We acknowledge the support of the Stuttgart Center for Simulation Science (SimTech). G.M. acknowledges the support of the grant RYC2022-035442-I funded by MCIN/AEI/10.13039/ 501100011033 and ESF+. G.M. also received support from the Japan Society for the Promotion of Science through its international fellow program (grant: P22013) and the Grant-inaid JP22F22013. P.R. thanks the financial support from the Spanish Ministerio de Ciencia e Innovación (PID2020-117742GB-I00). The authors acknowledge the support of the state of Baden-Württemberg through bwHPC and the German Research Foundation (DFG) through grant No INST 40/575-1 FUGG (JUSTUS 2 cluster) and the Research Center for Computational Science, Okazaki, Japan (Projects: 22-IMS-C301, 23-IMS-C128). G.M. also received support from project 20245AT016 (Proyectos Intramurales CSIC).

Facilities: bwHPC Justus Cluster (DE), RCCS (JP).

Software: Orca, v.5.0.4 (F. Neese et al. 2020; quantum chemical calculations), VMD, v.1.9.4 (W. Humphrey et al. 1996; J. Stone 1998; visualization and figure preparation), Chemcraft (Chemical structure manipulation and analysis) and Matplotlib v.3.6.3 (T. A. Caswell et al. 2023; article's plot preparation).

Appendix Benchmark of DFT Methods

Tables 4 and 5 show the activation energies of the 1,2 and 1,1 OH addition to vinyl alcohol for the syn isomer (syn-anti) in the gas phase using different DFT functionals (reactions R1 and R2). These were obtained after a full geometry optimization and corrected using the zero-point energy. We benchmarked our methods referencing the results for the same reaction in B. Ballotta et al. (2023). In their work, gas phase reactions on both isomers were performed. In this work, for computational saving reasons, we restrict our research to the case of syn- C_2H_3OH .

Table 4
Activation Energies $\Delta H^{\circ,\ddagger}$ for the OH Addition to C_2H_3OH Leading to HOC_2H_3OH Using Different Methods (kcal mol⁻¹)

Method	$\Delta H^{\circ,\ddagger}$
Reference (B. Ballotta et al. 2023)	1.0
BB1K/def2-TZVP	0.5
BHLYP-D3(BJ)/def2-TZVP	2.7
DSD-PBEP86-D3(BJ)/def2-TZVP	2.8
M06-2X-D3/def2-TZVP	1.6
M08-HX/def2-TZVP	1.1
MPWB1K-D3(BJ)/def2-TZVP	0.6
MPWKCIS1K/def2-TZVP	0.6
ω B97M-V/def2-TZVP	1.4

Table 5
Activation Energies $\Delta H^{\circ,\ddagger}$ for the OH Addition to C₂H₃OH Leading to C₂H₃(OH)₂ Using Different Methods (kcal mol⁻¹)

Method	$\Delta H^{\circ,\ddagger}$
Reference (B. Ballotta et al. 2023)	1.9
BB1K/def2-TZVP	1.8
BHLYP-D3(BJ)/def2-TZVP	4.1
DSD-PBEP86-D3(BJ)/def2-TZVP	3.9
M06-2X-D3/def2-TZVP	3.4
M08-HX/def2-TZVP	2.6
MPWB1K-D3(BJ)/def2-TZVP	1.8
MPWKCIS1K/def2-TZVP	2.3
ω B97M-V/def2-TZVP	1.2

In B. Ballotta et al. (2023), calculations are performed using Truhlar's calendar basis set Jun-cc-pVTZ (E. Papajak et al. 2011), which adds diffuse functions to the cc-pVTZ basis except to H, He and removes the highest angular momentum diffuse function from all other atoms. We opted for the 3ζ basis set def2-TZVP (F. Weigend & R. Ahlrichs 2005). We use the def2/J (F. Weigend 2006) and def2-TZVP/c (in the case of double hybrids, see below) auxiliary basis set for the resolution of the identity approximation (J. L. Whitten 1973; B. I. Dunlap et al. 1979).

Functionals were chosen to cover several existing families. We employed functionals designed for main group thermochemistry, thermochemical kinetics, and noncovalent interactions as well as more advanced hybrid functional approaches. The set is composed by BB1K (Y. Zhao et al. 2004), BHLYP (A. D. Becke 1993), DSD-PBEP86 (S. Kozuch & J. M. Martin 2011), M06-2X (Y. Zhao & D. G. Truhlar 2008a), M08-HX (Y. Zhao & D. G. Truhlar 2008b), MPWKCIS1K (Y. Zhao et al. 2005), MPWB1K (Y. Zhao & D. G. Truhlar 2004), ω B97M-V (N. Mardirossian & M. Head--Gordon 2016). We used dispersion corrections for functionals where such correction was parameterized, namely D3 (S. Grimme et al. 2010), D3(BJ; S. Grimme et al. 2011), or the correction by nonlocal correlation (NL; O. A. Vydrov & T. Van Voorhis 2010, included in ω B97M-V). The specific functionals for which we apply either correction or no correction at all can be consulted in Tables 4 and 5.

Considering the size of the ASW clusters, we chose the functional with the best cost/accuracy ratio. We discarded BHLYP-D3(BJ), DSD-PBEP86-D3(BJ), and M062-2X-D3

according to the constant overestimation of the barriers of both reactions. From the remaining functionals, we chose MPWB1K-D3(BJ)/def2-TZVP as the method for this study due to its good prediction for the barrier in Table 5. Though it may exhibit a relatively small error compared to the reference in Table 4, we considered it acceptable for the specific requirements of our study. The computational efficiency makes it overall a well-balanced choice considering the manageable computational cost associated with this method within our system.

ORCID iDs

Juan Carlos del Valle https://orcid.org/0000-0002-3251-3594

Pilar Redondo https://orcid.org/0000-0001-7876-4818

Johannes Kästner https://orcid.org/0000-0001-6178-7669

Germán Molpeceres https://orcid.org/0000-0001-8803-8684

References

```
Agúndez, M., Marcelino, N., Tercero, B., et al. 2021, A&A, 649, L4
Alvarez Barcia, S., Russ, P., Kästner, J., & Lamberts, T. 2018, MNRAS,
Andrés, D. S., Rivilla, V. M., Colzi, L., et al. 2024, ApJ, 967, 39
Ballotta, B., Martínez-Núñez, E., Rampino, S., & Barone, V. 2023, ESC, 7, 77
Becke, A. D. 1993, JChPh, 98, 7
Belloche, A., Garrod, R. T., Müller, H. S. P., et al. 2019, A&A, 628, A10
Belloche, A., Menten, K. M., Comito, C., et al. 2008, A&A, 492, 73
Belloche, A., Müller, H. S. P., Menten, K. M., Schilke, P., & Comito, C. 2013,
    &A, 559, A47
Beltrán, M. T., Codella, C., Viti, S., Neri, R., & Cesaroni, R. 2008, ApJ,
   690, L93
Butlerow, A. 1861, Justus Liebigs Annalen der Chemie, 120, 295
Caselli, P., Walmsley, C. M., Tafalla, M., Dore, L., & Myers, P. C. 1999, ApJ,
   523, L165
Caswell, T. A., Lee, A., Droettboom, M., et al. 2023, matplotlib/matplotlib:
   REL: v3.6.3, v3.6.3, Zenodo, doi:10.5281/zenodo.7527665
Cernicharo, J., Agúndez, M., Cabezas, C., et al. 2021, A&A, 649, L15
Cernicharo, J., Fuentetaja, R., Agúndez, M., et al. 2022, A&A, 663, L9
Chang, Q., & Herbst, E. 2016, ApJ, 819, 145
Coutens, A., Persson, M. V., Jørgensen, J. K., Wampfler, S. F., & Lykke, J. M.
   2015, A&A, 576, A5
Cuadrado, S., Goicoechea, J. R., Roncero, O., et al. 2016, A&A, 596, L1
Dunlap, B. I., Connolly, J. W., & Sabin, J. R. 1979, JChPh, 71, 402
Eckhardt, A. K., Linden, M. M., Wende, R. C., Bernhardt, B., &
   Schreiner, P. R. 2018, NatCh, 10, 1141
Etim, E. E., Gorai, P., Das, A., & Arunan, E. 2018, Ap&SS, 363, 6
Ferrero, S., Pantaleone, S., Ceccarelli, C., et al. 2023, ApJ, 944, 142
Ferrero, S., Zamirri, L., Ceccarelli, C., et al. 2020, ApJ, 904, 11
García de la Concepción, J., Colzi, L., Jiménez-Serra, I., et al. 2022, A&A,
  658, A150
García De La Concepción, J., Jiménez-Serra, I., Carlos Corchado, J.,
   Rivilla, V. M., & Martín-Pintado, J. 2021, ApJL, 912, L6
García De La Concepción, J., Jiménez-Serra, I., & Carlos Corchado, J. 2023,
   A&A, 675, A109
Garrod, R. T., Jin, M., Matis, K. A., et al. 2022, ApJS, 259, 1
Garrod, R. T., & Pauly, T. 2011, ApJ, 735, 15
Goto, M. 2014, in IAU Symp. 303, The galactic center: Feeding and feedback
  in a normal galactic nucleus (Cambridge: Cambridge Univ. Press), 429
Grimme, S., Antony, J., Ehrlich, S., & Krieg, H. 2010, JChPh, 132, 154104
Grimme, S., Ehrlich, S., & Goerigk, L. 2011, JCoCh, 32, 65
Hasegawa, T. I., & Herbst, E. 1993, MNRAS, 263, 589
Herbst, E., & van Dishoeck, E. F. 2009, ARA&A, 47, 427
Hollis, J. M., Lovas, F. J., Jewell, P. R., & Coudert, L. H. 2002, ApJ, 571, L59
Hollis, J. M., Lovas, F. J., & Jewell, P. R. 2000, ApJ, 540, L107
Humphrey, W., Dalke, A., & Schulten, K. 1996, Journal of Molecular
   Graphics, 14, 33
Ioppolo, S., Fedoseev, G., Chuang, K. J., et al. 2021, NatAs, 5, 197
Ishibashi, A., Hidaka, H., Oba, Y., Kouchi, A., & Watanabe, N. 2021, ApJL,
   921, L13
```

```
Jiménez-Serra, I., Rodríguez-Almeida, L., Martín-Pintado, J., et al. 2022,
   A&A, 663, A181
Jin, M., & Garrod, R. T. 2020, ApJS, 249, 26
Jørgensen, J. K., Favre, C., Bisschop, S. E., et al. 2012, ApJ, 757, L4
Kleimeier, N. F., Eckhardt, A. K., & Kaiser, R. I. 2021, JAChS, 143, 14009
Kozuch, S., & Martin, J. M. 2011, PCCP, 13, 20104
Kruse, H., & Grimme, S. 2012, JChPh, 136, 154101
Landau, L. D., & Lifshitz, E. M. 1976, Mechanics (3rd ed.; Oxford:
   Butterworth-Heinemann)
Lykke, J. M., Coutens, A., Jørgensen, J. K., et al. 2017, A&A, 597, A53
Mardirossian, N., & Head-Gordon, M. 2016, JChPh, 144, 214110
McGuire, B. A. 2018, ApJS, 239, 17
McGuire, B. A. 2022, ApJS, 259, 30
McGuire, B. A., Burkhardt, A. M., Kalenskii, S., et al. 2018, Sci, 359, 5
McGuire, B. A., Loomis, R. A., Burkhardt, A. M., et al. 2021, Sci, 371, 9
Melosso, M., Bizzocchi, L., Gazzeh, H., et al. 2022, Chem. Commun., 58, 3
Minissale, M., Congiu, E., Baouche, S., et al. 2013, PhRvL, 111, 053201
Minissale, M., Congiu, E., & Dulieu, F. 2016, A&A, 585, A146
Miyazaki, A., Tsuge, M., Hidaka, H., Nakai, Y., & Watanabe, N. 2022, ApJL,
   940, L2
Molpeceres, G., García De La Concepción, J., & Jiménez-Serra, I. 2021a, ApJ,
   923, 159
Molpeceres, G., Jiménez-Serra, I., Oba, Y., et al. 2022, A&A, 663, A41
Molpeceres, G., Kästner, J., Fedoseev, G., et al. 2021b, JPCL, 12, 10854
Molpeceres, G., & Rivilla, V. M. 2022, A&A, 665, A27
Molpeceres, G., Rivilla, V. M., Furuya, K., et al. 2023a, MNRAS, 521, 6061
Molpeceres, G., Zaverkin, V., Furuya, K., Aikawa, Y., & Kästner, J. 2023b,
    &A, 673, A51
Mullikin, E., Anderson, H., O'Hern, N., et al. 2021, ApJ, 910, 72
Neese, F., Wennmohs, F., Becker, U., & Riplinger, C. 2020, JChPh, 152,
  224108
Neese, F., Wennmohs, F., Hansen, A., & Becker, U. 2009, CP, 356, 109
Nonne, M., Melosso, M., Tonolo, F., et al. 2024, JPCA, 128, 4850
Pantaleone, S., Enrique-Romero, J., Ceccarelli, C., et al. 2020, ApJ, 897, 56
Pantaleone, S., Enrique-Romero, J., Ceccarelli, C., et al. 2021, ApJ, 917, 49
Papajak, E., Zheng, J., Xu, X., Leverentz, H. R., & Truhlar, D. G. 2011, JCTC,
   7, 34
Perrero, J., Enrique-Romero, J., Martínez-Bachs, B., et al. 2022, ESC, 6, 496
Rimola, A., Skouteris, D., Balucani, N., et al. 2018, ESC, 2, 720
Rivilla, V. M., Colzi, L., Jiménez-Serra, I., et al. 2022, ApJL, 929, L11
Rivilla, V. M., Jiménez-Serra, I., Martín-Pintado, J., et al. 2021, PNAS, 118,
   e2101314118
Rivilla, V. M., Martín-Pintado, J., Jiménez-Serra, I., et al. 2020, ApJ, 899, L28
Rocha, W. R. M., Van Dishoeck, E. F., Ressler, M. E., et al. 2024, A&A,
  683, A124
Rodler, M. 1985, JMoSp, 114, 30
Rodríguez-Almeida, L. F., Jiménez-Serra, I., Rivilla, V. M., et al. 2021, ApJL,
   912, L11
Ruaud, M., Wakelam, V., & Hersant, F. 2016, MNRAS, 459, 3756
Saito, S. 1976, CPL, 42, 402
Sanz-Novo, M., Rivilla, V. M., Jiménez-Serra, I., et al. 2023, ApJ, 954, 3
Sanz-Novo, M., Rivilla, V. M., Müller, H. S. P., et al. 2024, ApJ, 965, L26
Shapiro, R. 1988, OLEB, 18, 71
Shingledecker, C., Molpeceres, G., Rivilla, V., Majumdar, L., & Kästner, J.
   2020, ApJ, 897, 158
Shingledecker, C. N., Tennis, J., Gal, R. L., & Herbst, E. 2018, ApJ, 861, 20
Shingledecker, C. N., Vasyunin, A., Herbst, E., & Caselli, P. 2019, ApJ,
  876, 140
Stone, J. 1998, Master's thesis, Univ. Missouri-Rolla
Tinacci, L., Germain, A., Pantaleone, S., et al. 2023, ApJ, 951, 32
Vydrov, O. A., & Van Voorhis, T. 2010, JChPh, 133, 244103
Wakelam, V., Loison, J. C., Mereau, R., & Ruaud, M. 2017, MolAs, 6, 22
Weigend, F. 2006, PCCP, 8, 1057
Weigend, F., & Ahlrichs, R. 2005, PCCP, 7, 3297
Whitten, J. L. 1973, JChPh, 58, 501
Zaverkin, V., Molpeceres, G., & Kästner, J. 2022, MNRAS, 510, 3063
Zeng, S., Jiménez-Serra, I., Rivilla, V. M., et al. 2021, ApJL, 920, L27
Zeng, S., Quénard, D., Jiménez-Serra, I., et al. 2019, MNRAS: Letters,
   484, L43
Zeng, S., Zhang, Q., Jiménez-Serra, I., et al. 2020, MNRAS, 497, 4896
Zhao, Y., González-García, N., & Truhlar, D. G. 2005, JPCA, 109, 8
Zhao, Y., Lynch, B. J., & Truhlar, D. G. 2004, JPCA, 108, 9
Zhao, Y., & Truhlar, D. G. 2004, JPCA, 108, 18
Zhao, Y., & Truhlar, D. G. 2005, JPCA, 109, 5656
Zhao, Y., & Truhlar, D. G. 2008a, Theor. Chem. Acc., 120, 215
Zhao, Y., & Truhlar, D. G. 2008b, JCTC, 4, 68
```